

Judicious Heteroatom Doping Produces High Performance Deep Blue Multiresonant Thermally Activated Delayed Fluorescence Organic Light-Emitting Diodes

Subeesh Madayanad Suresh,^{a,†} Le Zhang,^{a,b,‡} Tomas Matulaitis,^a David Hall,^{a,d} Changfeng Si,^a Alexandra M. Z. Slawin,^a Stuart Warriner,^c David Beljonne,^d Yoann Olivier,^{d,e} Ifor D. Samuel^{*b} and Eli Zysman-Colman^{*a}

^aOrganic Semiconductor Centre, EaStCHEM School of Chemistry, University of St Andrews, St Andrews, UK, KY16 9ST. E-mail: eli.zysman-colman@st-andrews.ac.uk

^bOrganic Semiconductor Centre, SUPA School of Physics and Astronomy
University of St Andrews, St Andrews KY16 9SS, UK

^cSchool of Chemistry, University of Leeds, Woodhouse Lane, Leeds, UK

^dLaboratory for Chemistry of Novel Materials, University of Mons, 7000, Mons, Belgium.

^eLaboratory for Computational Modeling of Functional Materials, Namur Institute of Structured Matter, Université de Namur, Rue de Bruxelles, 61, 5000 Namur, Belgium.

[†] These authors contributed equally

Abstract

We show how borylation of an acceptor-donor-acceptor (A-D-A) thermally activated delayed fluorescence (TADF) emitter, **DIDOBNA-N**, transforms the compound into a multi-resonant TADF (MR-TADF) emitter, **MesB-DIDOBNA-N**. **DIDOBNA-N** emits bright blue light ($\lambda_{\text{PL}} = 444$ nm, FWHM = 64 nm, $\Phi_{\text{PL}} = 81\%$, $\tau_{\text{d}} = 23$ μs , 1.5 wt% in TSP01). The deep blue organic light-emitting diode (OLED) based on this compound shows a very high maximum external quantum efficiency (EQE_{max}) of 15.3% for a device with CIE_y of 0.073. The MR-TADF emitter, **MesB-DIDOBNA-N** shows efficient and narrowband violet emission ($\lambda_{\text{PL}} = 402$ nm, FWHM = 19 nm, $\Phi_{\text{PL}} = 74.7\%$, $\tau_{\text{d}} = 133$ μs , 1.5 wt% in TSP01). The OLED with **MesB-DIDOBNA-N** shows outstanding efficiency for a violet OLED at 9.3% and $\text{CIE}_y = 0.044$, which is the bluest EL reported for a MR-TADF OLED to date. Noteworthy are the CIE coordinates of (0.166, 0.045), which are very close to the Rec.2020 standard for blue (0.131,

0.046). The EQE_{max} values were improved from 9.3% to 13.6% by increasing the concentration of the emitter in the host from 1.5 wt% to 5 wt%.

Introduction

Organic light-emitting diodes (OLEDs) are rapidly becoming the preferred display technology for a range of consumer electronics, from smartwatches, mobile phones and laptops to large screen televisions and displays used in the automotive industry.¹ Ultra-high-definition displays must meet ever more stringent industry color standards, the most recent of which being Rec 2020., which are defined according to the Commission International de l'Éclairage (CIE) 1931 as (0.131, 0.046), (0.17, 0.797) and (0.708, 0.292) for blue, green, and red, respectively.² Presently commercial vacuum-deposited OLEDs rely on phosphorescent complexes as emitter materials for the red and green sub-pixels and organic fluorescent materials for the blue sub-pixel. Significant research has been devoted to developing sustainable organic emitters that operate at comparable efficiencies to phosphorescent complexes and so can replace noble metal-based emitters for red and green OLEDs, and for blue OLEDs can lead to much higher efficient devices.^{3, 4} Organic compounds that exhibit thermally activated delayed fluorescence (TADF) have the most potential to act as replacement emitters in OLEDs as this class of material can harvest 100% of the electrically generated excitons and convert these to light emission.^{5, 6} Though TADF OLEDs now show comparable efficiencies to phosphorescent OLEDs for each of the red, green and blue devices, the typically employed donor-acceptor design results in emission from a charge-transfer (CT) state that is broad and unstructured, leading to poor chromaticity in the device. A subclass of TADF emitters, multi-resonant TADF (MR-TADF), however, shows great promise to address the issue of colour purity. MR-TADF emitters show very narrowband emission (full width half maximum, FWHM <40 nm),⁷ which is due to their very rigid polycyclic aromatic structure and their short range charge transfer (SRCT) excited state.^{8, 9} Their use in OLEDs would obviate the need for the use of color filters, leading to more energy efficient devices.

Since the first report of an MR-TADF compound from the group of Hatakeyama, over two hundred separate MR-TADF materials have been identified as hosts or emitters for OLEDs,^{8, 10} with examples

of their use in high-efficiency blue, green and red OLEDs. Near UV and violet emitters for OLEDs are one class where there is a dearth of reports.¹¹ Potential uses of short wavelength OLEDs are for sensing,¹² photocopying,¹³ high density information storage¹⁴ and sterilization.¹⁵ Most of the reported efficient near UV OLEDs (<400 nm) using purely organic emitters¹¹ to date contain materials that emit from a hybridized local and charge transfer excited state (HLCT)^{16, 17} where triplets are harvested through a hot exciton channel mechanism involving reverse intersystem crossing (RISC) from higher lying triplet (T_n) states to S_1 .¹⁸ A recent report from Tang *et al.* demonstrated record setting performance values for an HLCT emitter-based near UV-OLED [$\lambda_{EL} = 396$ nm, $EQE_{max} = 10.79\%$, CIE (0.161, 0.031)].^{8, 11, 16} There are also a small number of reports of near UV TADF and MR-TADF emitters and their use in OLEDs (Figure 1).¹⁰ The first report of a near UV-emitting MR-TADF compound is based on a boron, oxygen doped triangulene type structure reported by Hatakeyama, **2a**¹⁹ ($\lambda_{PL} = 398$ nm, FWHM = 33 nm, $\Delta E_{ST} = 0.18$ eV, $\tau_D = 66$ μ s in 1wt% PMMA).²⁰ This compound, also known as **DOBNA**, was initially identified as a potential host material due to its large band gap and high triplet energy. In the same report, phenyl derivatives of **2a** were employed as host materials in phosphorescent OLEDs.¹⁹ Other reports have mostly documented the use of the DOBNA fragment as a weak acceptor in D-A type violet²¹ ($\lambda_{PL} < 450$ nm) TADF emitters.⁸ In 2015, Kwon *et al.* reported two deep blue emitters containing the DOBNA fragment as the acceptor.²² The OLED with the acridine donor-based emitter, **TDBA-Ac** presented an EQE_{max} of 21.5% and an excellent CIE_y of 0.06. Choi *et al.* reported devices using related tercarbazole donor-based **TB-3Cz** and **TB-P3Cz** emitters that showed EQE_{max} of 9.9% and 6.1%, respectively, with corresponding CIE_y values were 0.07 and 0.08, respectively for **TB-3Cz** and **TB-P3Cz**.²³ A structurally related deep blue emitter containing a spiroacridan donor was reported by Kim *et al.*, **TDBA-SAF**-based device achieved an EQE_{max} of 28.2% and a CIE_y of 0.09.²⁴ Recently, Choi *et al.* reported two deep blue solution-processible emitters containing extended carbazole donor units connected to DOBNA acceptor, **BO-tCzPhICz** and **BO-tCzDICz**. The solution-processed OLEDs showed EQE_{max} of 17.8% and 14.8%, respectively, and with CIE_y of 0.07 and 0.062, respectively.²⁵ Hong *et al.* reported two tri-spiral acridine donor based blue emitters, **OBOtSAC** and **tBuOBOtSAC** and their use in OLEDs.²⁶ Both emitters showed efficient (Φ_{PL} above 90%) deep blue

emission at 452nm (FWHM = 50 nm) and 446 nm (FWHM = 48 nm), respectively for **OBOtSAc** and **tBuOBOtSAc**. Both devices achieved very high EQE_{max} of 31.2% and 28.2% with CIE_y of 0.092 and 0.061, respectively. Tong *et al.* reported OLEDs using two deep blue emitters **TDBA-PAS** and **TDBA-DPAC** that can achieve EQE_{max} of 22.4% and 24.6% at CIE_y of 0.042 and 0.085, respectively.²⁷ These two emitters each show two different conformers in the solid state and the authors contend that one conformer acts as a host for the other, evidenced by the improved performance in the device at high doping concentrations (≤ 50 wt%). Su *et al.* reported a disk-like emitter based on a DOBNA acceptor decorated with three diphenylamine units, **BO3N**, which showed narrowband blue emission ($\lambda_{\text{PL}} = 424$ nm, FWHM = 34 nm) with high Φ_{PL} of 80% in toluene solution. The OLED with the emitter **BO3N** showed an EQE_{max} of 10.4% and CIE_y value of 0.08.²⁸

The DOBNA fragment has thus been shown to be a promising motif used in the construction of D-A type efficient deep blue TADF emitters. An alternative design for UV emitters was highlighted by Lee *et al.* where they reported a fused indolocarbazole (**tDIDCz**) derivative that presented incredibly narrowband EL (FWHM = 14 nm, $\lambda_{\text{EL}} = 401$ nm) with CIE coordinates of (0.164, 0.018) in the device.²⁹ Though this compound shows the characteristic pattern of alternating increasing and decreasing electron density on adjacent atoms in the excited state, the ΔE_{ST} of 0.44 eV is too large due to the very different natures of the S_1 and T_1 excited states resulting in the absence of delayed fluorescence.³⁰ The absence of triplet harvesting in the OLED limited the EQE_{max} to only 2.75% (Table S7).

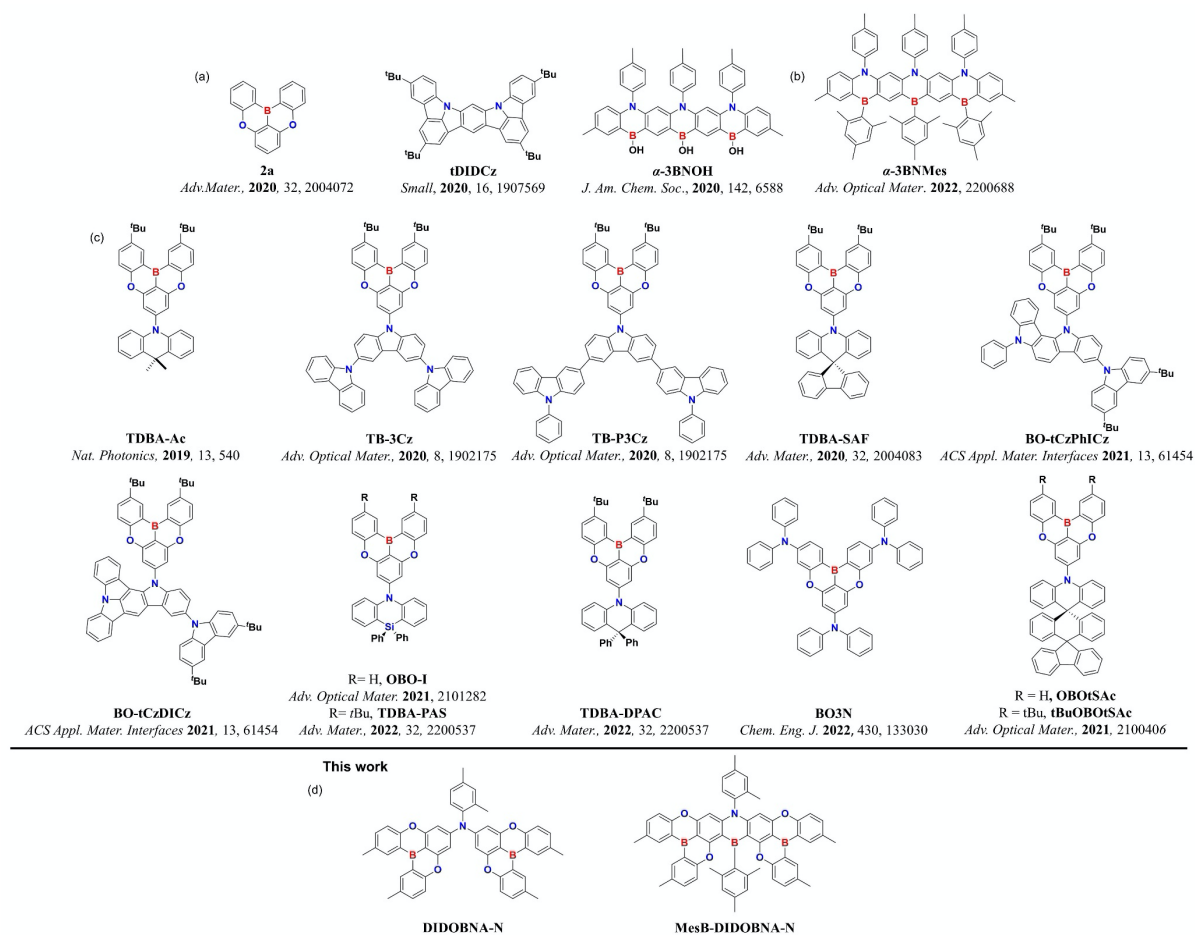


Figure 1. (a) Chemical structures of previously reported violet MR-TADF emitters (b) α -3BNMes, (c) D-A TADF emitters with $CIE_y \leq 0.1$ with DOBNA acceptor fragment, and (d) chemical structures of our molecules.

In 2020, we reported a near UV emitting linear ladder type B,N-doped heptacene (Figure 1), α -3BNOH ($\lambda_{PL} = 390$ nm, FWHM = 31 nm, $\Delta E_{ST} = 0.31$ eV in THF) that showed an emission resulting from TADF and TTA and narrow deep blue emission in solution.³¹ By replacing the OH group attached to boron with mesityl units in α -3BNOH, a red shift of the emission was observed for α -3BNMes ($\lambda_{PL} = 443$ nm, FWHM = 30 nm, THF, $\Delta E_{ST} = 0.28$ eV, 1 wt% in PMMA).³² Here, we report two emitters, one based on an A-D-A design containing two DOBNA acceptor groups that emits in the deep blue (**DIDOBNA-N**), and a second B,N,O doped heptacene MR-TADF compound that emits in the near UV (**MesB-DIDOBNA-N**). Both compounds exhibit weak TADF due to their moderately large ΔE_{ST} of 0.23 and 0.24 eV yet demonstrate high Φ_{PL} of 81 and 75% for **DIDOBNA-N** and **MesB-DIDOBNA-N**, respectively. The OLED with **DIDOBNA-N** showed deep blue emission at 444 nm (FWHM = 64 nm) corresponding to CIE coordinates of (0.152, 0.073) with an EQE_{max} of 15.2%. The OLED with

MesB-DIDOBNA-N showed near UV emission with λ_{EL} of 401 nm, FWHM = 22 nm, corresponding to CIE coordinates of (0.165, 0.044). By increasing the doping concentration of **MesB-DIDOBNA-N** in the emitting layer of the device, from 1.5 wt% to 3 wt% and 5 wt%, the EQE_{max} increased from 9.3%, 11.3% and 13.6% respectively. Only minor variances were observed in the emission maxima and CIE_y value with increasing doping concentration. The EQE_{max} value of the 5 wt% doped device represents the most efficient device among those employing purely organic violet emitters.^{10, 11}

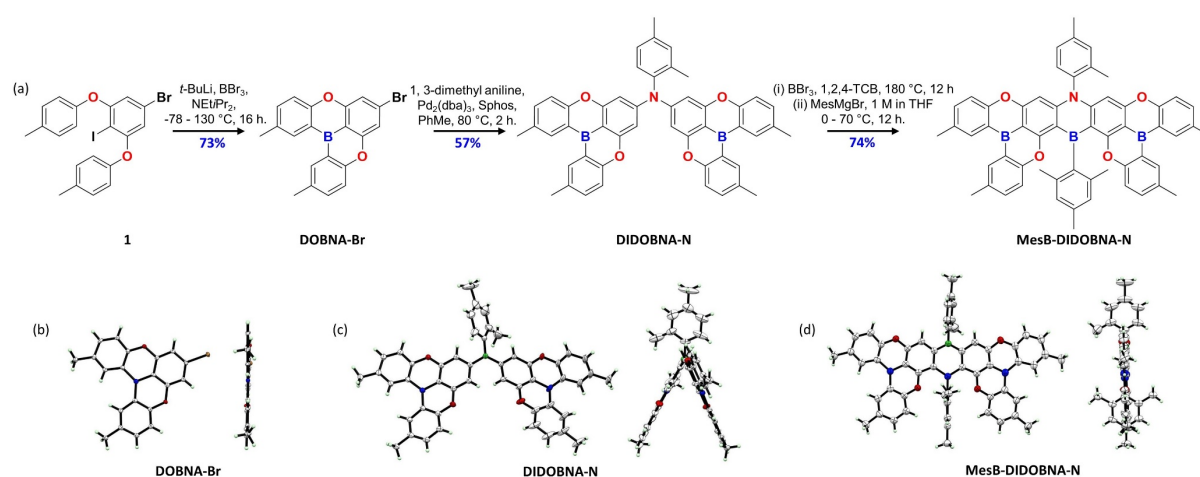


Figure 2. (a) Synthesis of target emitters. ORTEP diagram of compounds, and their side views of (b) **Br-DOBNA** (c) **DIDOBNA-N** and (d) **MesB-DIDOBNA-N**. Thermal ellipsoids are displayed at the 50% probability level.

Results and Discussion

MesB-DIDOBNA-N was obtained in three steps from compound **1** (Figure 2). **DOBNA-Br**, a key intermediate, was obtained through a sequence of S_NAr and electrophilic borylation in good yield; the borylation reaction proceeded in 73% yield. **DIDOBNA-N** was obtained in 57% yield following a Buchwald-Hartwig cross-coupling reaction of two equivalents of **DOBNA-Br** with 2,4-dimethylaniline. **DIDOBNA-N** was then subjected to electrophilic borylation with BBr_3 and quenching with MesMgBr to afford **MesB-DIDOBNA-N** in 74% yield. The identity and purity of the synthesized molecules were established from a combination of ^1H and ^{13}C NMR spectroscopy, high-resolution mass spectrometry (HRMS), elemental analysis (EA), and gel permeation chromatography (GPC) (Figures S1-S15)

Single crystals of **DOBNA-Br** were obtained directly from the reaction mixture. **DIDOBNA-N** crystals were obtained following temperature-gradient sublimation, and **MesB-DIDOBNA-N** were obtained by slow diffusion of hexane into saturated solution of the emitter in THF. Their structures are shown in Figure 2b-d. No intermolecular hydrogen bonding or π - π stacking interactions were observed for **DIDOBNA-N** and **MesB-DIDOBNA-N**. In **MesB-DIDOBNA-N**, the B-C_{Mes} bond is longer [1.587(3) Å] than the B-C bonds within the DOBNA fragment [1.536(3) and 1.540(3) Å], a structural feature previously observed in other compounds containing a mesitylated borane.³³ This emitter has a planar structure and the two aryl moieties attached to the B and N positioned are oriented approximately orthogonal to the acene core.

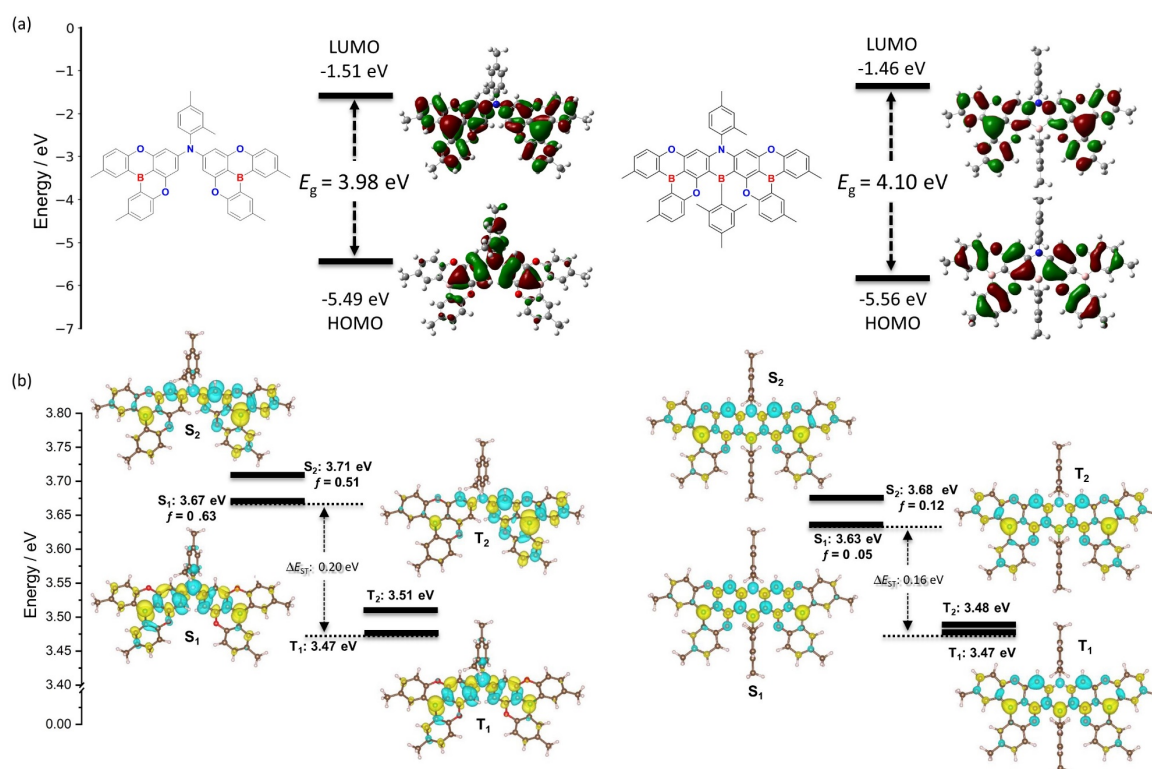


Figure 3. **a)** HOMO and LUMO electron density distribution and orbital energies of **DIDOBNA-N** and **MesB-DIDOBNA-N** calculated at PBE0/6-31G(d,p) in the gas phase, isovalue = 0.02; **b)** Difference density plots and energies for the lowest two lying singlet and triplet excited states for **DIDOBNA-N** and **MesB-DIDOBNA-N** calculated at SCS-CC2/cc-pVDZ in the gas phase (isovalue = 0.001). Blue color represents an area of decreased electron density, and yellow represents an increased electron density between the ground and excited states. f denotes the oscillator strength for the transition to the excited singlet state

We then undertook a computational study to understand the ground and excited state properties of **MesB-DIDOBNA-N** as well as the A-D-A system **DIDOBNA-N** (Figure 3). Ground state calculations were carried out using Density Functional Theory (DFT) at the PBE0/6-31G(d,p) level in the gas phase. The DFT calculations predict a 0.12 eV increase in the band gap from **DIDOBNA-N** to **MesB-DIDOBNA-N**, despite the apparent increase in conjugation length. Both **DIDOBNA-N** and **MesB-DIDOBNA-N** display similar electron density distribution patterns for their LUMOs, with a pattern that is reminiscent of the DOBNA moiety¹⁹ (Figure S16). However, **DIDOBNA-N** and **MesB-DIDOBNA-N** show distinct electron density distribution patterns for their HOMOs. The electron density of the HOMO in **DIDOBNA-N** is reminiscent of triphenylamine, a good electron donor, while the electron density of the HOMO in **MesB-DIDOBNA-N** is localized on the DOBNA units, similar to the DOBNA core,¹⁹ and with a nodal plane passing through the central nitrogen and boron atoms of the molecule. Excited state calculations were performed using wavefunction based methods using the spin-component scaling second-order approximate coupled-cluster (SCS-CC2) in tandem with the cc-pVDZ basis set, which we have previously shown to be a sufficient level of theory to accurately predict ΔE_{ST} in MR-TADF emitters.³⁴ The S_1 energy of **DIDOBNA-N** of 3.67 eV is slightly higher than that of **MesB-DIDOBNA-N** at 3.63 eV. Despite their similar S_1 energies, the oscillator strengths (f) for the S_0 - S_1 transition are starkly different at 0.63 and 0.05 for **DIDOBNA-N** and **MesB-DIDOBNA-N**, respectively. The much-attenuated f in **MesB-DIDOBNA-N** is likely the result of the higher symmetry of this compound (Figure S17). Notably, a similar change in the properties of the singlet excited state was predicted for **DABNA-1** compared to its more symmetric fused derivative **TABNA**.³⁴ Identical T_1 energies of 3.47 eV were predicted for **DIDOBNA-N** and **MesB-DIDOBNA-N**, resulting in ΔE_{ST} of 0.20 eV and 0.16 eV, respectively. An intermediate triplet state was predicted to exist in both compounds, which is acknowledged to facilitate RISC via spin-vibronic coupling in D-A TADF emitters.^{34, 35, 36, 37,}

³⁸ Difference density plots of the S_1 , S_2 , T_1 and T_2 states are shown in Figure 2b. For **MesB-DIDOBNA-N** each excited state possesses the typical alternating pattern of increasing and decreasing electron density of MR-TADF compounds that is characteristic of an excited state possessing SRCT character. The magnitude of the CT character of the excited state was quantified using two separate metrics: (1) the distance of charge transfer (D_{CT}) and (2) the amount of charge transferred (q_{CT}). These two metrics

reveal that there is a greater CT character in the excited states of **DIDOBNA-N** compared to that of **MesB-DIDOBNA-N** (Tables S1-3), pointing towards a more distinct long-range charge transfer (LRCT) character for the former compound; however, the magnitude of the CT character of **DIDOBNA-N** is still modest compared to conventional D-A TADF emitters, with D_{CT} reported to be 1.1 Å here while typical D-A TADF emitters show D_{CT} of > 1.6 Å.³⁹ Notably, the orbital types for the T_2 states of both compounds are different from those of S_1 and so spin-orbit coupling is expected to be non-negligible.

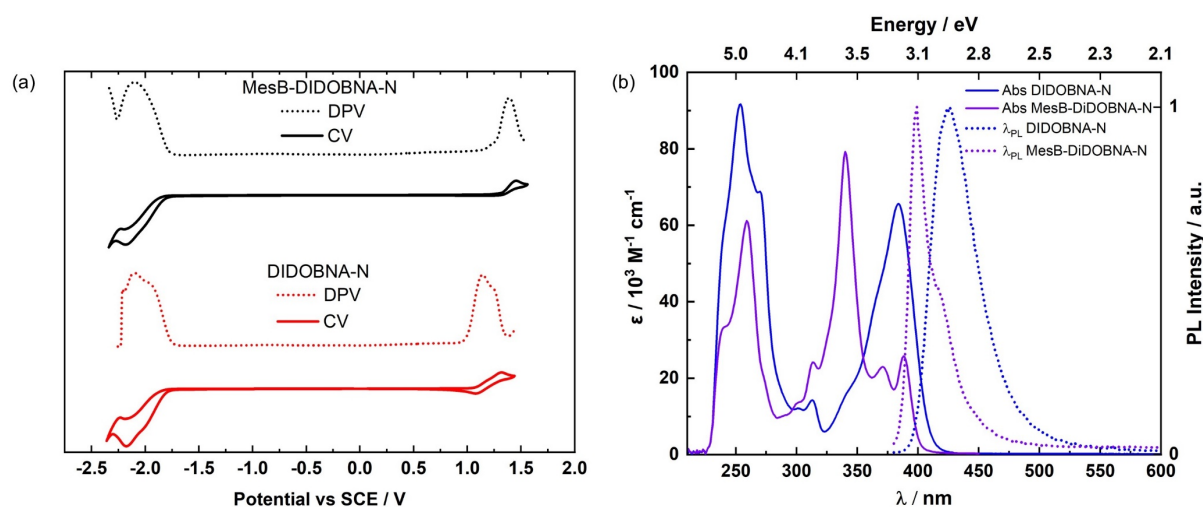


Figure 4. (a) Cyclic and differential pulse voltammograms measured in degassed DCM with 0.1 M $[n\text{Bu}_4\text{N}]\text{PF}_6$ as the supporting electrolyte and Fc^+/Fc as the internal reference (0.46 V vs SCE).⁴⁰ Scan rate = 50 mV s^{-1} . (b) Solution-state absorption and steady-state emission spectra at 300 K measured in THF. $\lambda_{\text{exc}} = 365 \text{ nm}$.

The electrochemical properties of both emitters were investigated by cyclic voltammetry (CV) and differential pulse voltammetry (DPV) in deaerated DCM with 0.1 M tetra-*n*-butylammonium hexafluorophosphate as the supporting electrolyte (Figure 4a). The oxidation potential, E_{ox} , determined from the peak value of the first oxidation wave of the DPV curve is 1.14 V and 1.39 V vs SCE, respectively, for **DIDOBNA-N** and **MesB-DIDOBNA-N**, which translate to respective HOMO levels of -5.48 eV and -5.73 eV. This is in line with the DFT calculations that predict a stabilization of the HOMO energy level of **MesB-DIDOBNA-N** compared to **DIDOBNA-N**. For **DIDOBNA-N**, there was a second oxidation peak in the DPV at 1.25 V. The reduction potential, E_{red} , determined from the peak value of the first reduction wave of the DPV curve is -1.94 V and -2.10 V vs SCE, respectively, for **DIDOBNA-N** and

MesB-DIDOBNA-N, which correspond to respective LUMO levels of -2.40 eV and -2.24 eV. The DFT calculations corroborate the trend in LUMO levels. The LUMO energy level of **DIDOBNA-N** is similar to other reported D-A type deep blue emitters having a DOBNA fragment as the acceptor.^{22, 25, 41, 42} Reductions for both emitters were broad, in the case of **DIDOBNA-N** a second reduction peak appeared at -2.10 V, which is likely due to the reduction of second DOBNA unit. The electrochemical band gap is calculated to be 3.08 eV and 3.49 eV, respectively for **DIDOBNA-N** and **MesB-DIDOBNA-N**. Moving from **DIDOBNA-N** to **MesB-DIDOBNA-N**, the addition of the B-Mes unit resulted in a destabilization of the LUMO by 0.16 eV and a stabilization of the HOMO by 0.25 eV. The increasing band gap from **DIDOBNA-N** to **MesB-DIDOBNA-N** is consistent with the trend predicted by DFT.

Table 1. Photophysical properties of **DIDOBNA-N** and **MesB-DIDOBNA-N**.

Compound	Medium	λ_{Abs}^c / nm	λ_{PL}^d / nm	FWHM ^e / nm	$E_{\text{S}_1}^f$ / eV	$E_{\text{T}_1}^f$ / eV	$\Delta E_{\text{S}_1^h}$ / eV	Φ_{PL}^i / %	τ_{P}^j / ns	τ_{D}^j / μs	k_{ISC}^k / s^{-1}	k_{RISC}^k / s^{-1}	$k_{\text{s,r}}^k$ / s^{-1}	$k_{\text{s,nr}}^k$ / s^{-1}
DIDOBNA-N	Sol. ^a	384 (66)	426	43	3.08 _g	2.86 _g	0.22	75 ^a	3.07	-	-	-	-	-
	film ^b	-	444	64	3.12	2.89	0.23	80.8 _b	6.83	13.7	1.55×10^7	3.14×10^4	1.19×10^8	2.77×10^7
MesB-DIDOBNA-N	Sol. ^a	388 (26)	399	23	3.17 _g	2.93 _g	0.24	33 ^a	2.63	-	-	-	-	-
	film ^b	-	402	19	3.18	2.94	0.24	74.7 _b	5.09	95.9	6.18×10^7	9.81×10^3	1.47×10^8	4.97×10^7

^aIn THF solutions (10^{-6} M). ^bMeasured in evaporated thin films consisting of 1.5 wt% emitter in TSPO1 host under vacuum. $\lambda_{\text{exc}} = 280$ nm. ^cLowest energy absorbance peak, Absorptivity (ϵ) in parenthesis ($/10^4 \text{ M}^{-1} \text{ cm}^{-1}$). ^dSteady-state emission maximum at 300 K. $\lambda_{\text{exc}} = 365$ nm. ^eFull width at half maximum of emission peak. ^f S_1 and T_1 energies were obtained from the onsets of the respective prompt fluorescence (delay: 1 ns; gate time: 100 ns) and phosphorescence spectra (delay: 1 ms; gate time: 9 ms) at 77 K. $\lambda_{\text{exc}} = 343$ nm. ^gSolution samples for ΔE_{ST} measurements were prepared in 2-MeTHF (10^{-6} M). ^h $\Delta E_{\text{ST}} = E(S_1) - E(T_1)$. ⁱRelative Φ_{PL} in solutions were measured by a comparative method using quinine sulfate as a standard ($\Phi_{\text{r}} = 54.6\%$ in 1 N H_2SO_4),⁴³ while absolute Φ_{PL} of the thin films were measured using an integrating sphere. ^jPrompt and delayed lifetimes were obtained by TCSPC and MCS, respectively. $\lambda_{\text{exc}} = 378$ nm. ^kIntersystem and reverse intersystem crossing rates were calculated using steady-state approximation method as described in literature.⁴⁴

The photophysical properties were studied by measurements of absorption and photoluminescence (PL), PL quantum yield (Φ_{PL}) and time-resolved PL in 10^{-6} M THF. Figure 4b shows the absorption and PL properties of **DIDOBNA-N** and **MesB-DIDOBNA-N** and these together with other photophysical data are collated in Table 1. There is excellent agreement between the experimental and simulated

absorption spectra (Figure S17). Intense absorption bands were noted for **DIDOBNA-N** and **MesB-DIDOBNA-N** around 250 nm, reflected in the molar absorptivity (ϵ) values of $92 \times 10^4 \text{ M}^{-1} \text{ cm}^{-1}$ and $50 \times 10^4 \text{ M}^{-1} \text{ cm}^{-1}$, respectively. An intense band at 340 nm ($\epsilon = 79 \times 10^4 \text{ M}^{-1} \text{ cm}^{-1}$) was observed for **MesB-DIDOBNA-N**, which has a similar alternating increasing/decreasing electron density pattern to S_1 that is indicative of a SRCT state (Figure S17). For **DIDOBNA-N** there is an intense band at 384 nm ($\epsilon = 66 \times 10^4 \text{ M}^{-1} \text{ cm}^{-1}$), a feature also observed in the absorption spectra of other D-A systems containing DOBNA acceptor fragment.^{22, 24, 41} The lowest energy absorption band in **DIDOBNA-N** is blue-shifted compared to that in **MesB-DIDOBNA-N**, which aligns with the predicted SCS-CC2 calculations (*vide supra*). The intensity at the lowest energy absorption band is higher for **DIDOBNA-N** than **MesB-DIDOBNA-N**. This is qualitatively consistent with the predicted higher oscillator strength of S_1 and S_2 of **DIDOBNA-N** compared to those of **MesB-DIDOBNA-N**, where the oscillator strength is weak (<0.1) for S_1 .

The PL spectra in solution state at RT reveal deep-blue and near UV emission (Figure 4b) for **DIDOBNA-N** and **MesB-DIDOBNA-N**, respectively. **DIDOBNA-N** shows an unstructured emission peaking at $\lambda_{\text{PL}} = 426 \text{ nm}$ and a moderate FWHM of 43 nm (0.29 eV). The emission from this compound is among the bluest D-A compounds containing a DOBNA acceptor moiety.^{22, 23, 24, 25, 26, 27, 28, 45} **MesB-DIDOBNA-N** emits in the violet at $\lambda_{\text{PL}} = 399 \text{ nm}$, with a very small FWHM of 23 nm (0.17 eV); and a low energy shoulder at 417 nm. This emission is narrower than that reported for **DOBNA** ($\lambda_{\text{PL}} = 398 \text{ nm}$, FWHM = 34 nm in DCM, Figure 1).¹⁹ The Stokes shifts of **DIDOBNA-N** and **MesB-DIDOBNA-N** are 42 nm and 11 nm, respectively, reflecting the small reorganization energies in the excited states of these two compounds, especially for the MR-TADF emitter. The singlet-triplet energy gaps (ΔE_{ST}), determined from the difference in energy of the onsets of the prompt fluorescence and phosphorescence spectra at 77 K in 2Me-THF glass (Figure S18) are 0.22 eV and 0.24 eV, respectively, for **DIDOBNA-N** and **MesB-DIDOBNA-N**, values in line with the predicted ones (Figure 3b). **DIDOBNA-N** and **MesB-DIDOBNA-N** possess similar triplet energy levels of 2.86 eV and 2.93 eV, respectively. The Φ_{PL} in degassed dilute THF solutions are 75% and 33% for **DIDOBNA-N** and **MesB-DIDOBNA-N**,

respectively. The Φ_{PL} values decrease to 61% and 26%, respectively, upon exposure to air. Both emitters showed a small decrease in Φ_{PL} upon exposure to air that can be attributed to singlet quenching⁴⁶ as there was no delayed emission detected in the transient PL measurements (Figure S19).

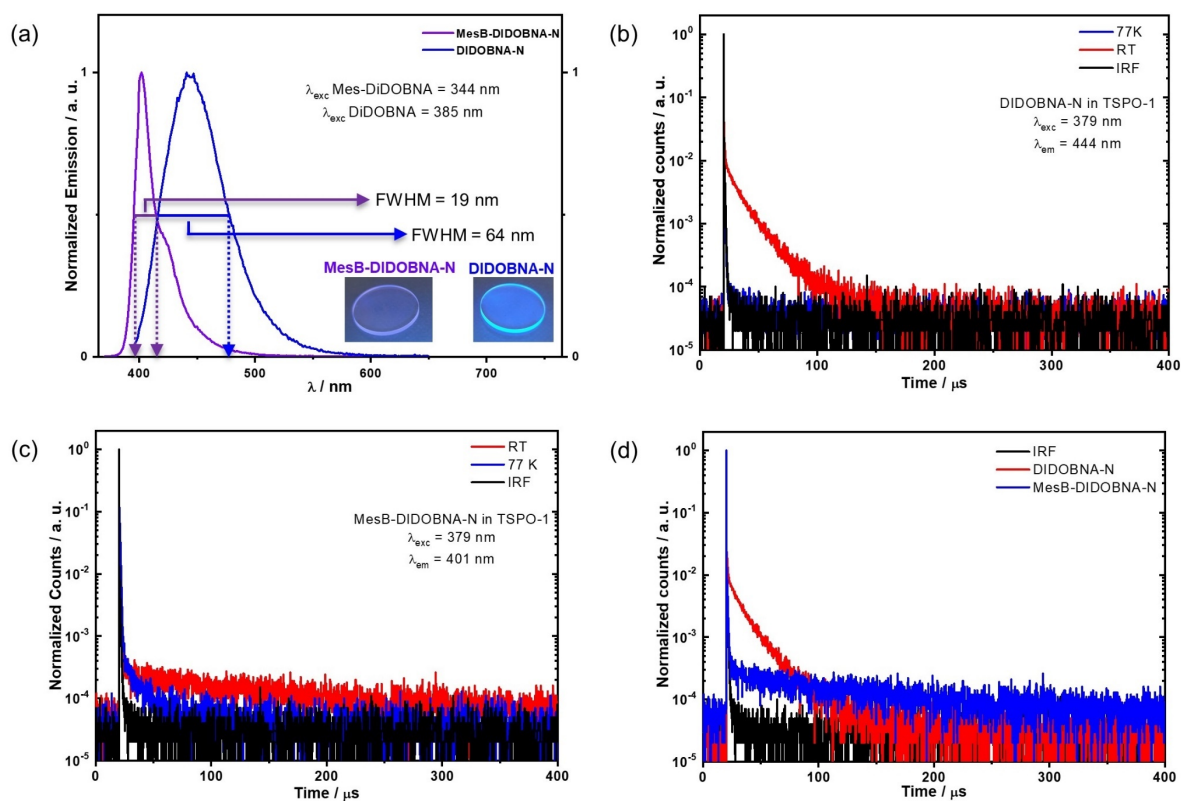


Figure 5. Co-evaporated thin film of 1.5 wt% emitter in TSPO1. **a)** Steady-state PL spectra at room temperature under vacuum, $\lambda_{\text{exc.}}(\text{DIDOBNA-N}) = 385 \text{ nm}$, $\lambda_{\text{exc.}}(\text{MesB-DIDOBNA-N}) = 344 \text{ nm}$; **b)** Time-resolved PL decay at RT and 77 K of **DIDOBNA-N**, $\lambda_{\text{exc.}} = 379 \text{ nm}$; **c)** Time-resolved PL decay at RT and 77 K of **MesB-DIDOBNA-N**, $\lambda_{\text{exc.}} = 379 \text{ nm}$; **d)** Decay of emission signal at RT plotted together with IRF signal.

To avoid possible intermolecular interactions or concentration-induced quenching, both molecules were doped into high triplet energy (E_{T}) hosts at a low doping concentration. Three high triplet energy widely used phosphine-oxide-based hosts, TSPO1, DPEPO, and PPT, were compared, among which TSPO1 showed the best performance in terms of Φ_{PL} (Table S6) and device EQE that are due to its high E_{T} (3.36 eV) and tendency to better bipolar carrier transport than the other host materials.⁴⁷ The Φ_{PL} values for 1.5 wt% doped TSPO1 films containing **DIDOBNA-N** and **MesB-DIDOBNA-N** are 81% and 75%, respectively (Table S6). Figure 5a shows the steady state photophysical properties of evaporated thin

films with a doping concentration of 1.5 wt% in TSPO1. **DIDOBNA-N** shows a deep blue emission at 444 nm with FWHM of 64 nm (0.38 eV), which is red-shifted and broader than that in dilute THF solution [$\lambda_{\text{PL}} = 426$ nm and FWHM = 43 nm (0.29 eV)]. The red-shift and spectral broadening of the emission are attributed to the polarization effect of the host matrix on the different excited state properties as CT-type TADF emitters are sensitive to the host polarity.^{48, 49} By contrast, **MesB-DIDOBNA-N** showed negligible changes in its steady-state PL spectrum in the thin film [λ_{PL} at 402 nm and a FWHM of only 19 nm (0.15 eV)] compared to that in solution [$\lambda_{\text{PL}} = 399$ nm and FWHM = 23 nm (0.17 eV)]. The observed narrowband emission spectra of **DIDOBNA-N** and **MesB-DIDOBNA-N** translate to deep blue and violet emission at Commission Internationale de l'Éclairage (CIE) coordinates of (0.150, 0.063), and (0.165, 0.022), respectively, which match well the blue CIE coordinates of BT.709 and BT.2020 standards for HDTV and UHDTV, i.e., (0.150, 0.06), and (0.131, 0.046), respectively. The S_1/T_1 energies for **DIDOBNA-N** and **MesB-DIDOBNA-N** in 1.5 wt% doped TSPO1 films were determined from the onsets of the respective prompt fluorescence and phosphorescence spectra at 77 K, which are 3.12 eV/2.89 eV and 3.18 eV/2.94 eV, respectively. The corresponding ΔE_{ST} values are 0.23 eV and 0.24 eV, respectively, which are consistent with those determined in 2-MeTHF.

We next acquired temperature-dependent time-resolved PL decays of the TSPO1 doped films using multi-channel scaling (MCS). The decays, which are presented in Figures **5b-c**, show both prompt (PF) and delayed fluorescence (DF) components for both emitters. Whereas the prompt component exhibited negligible temperature dependence, the intensity of the DF decreased significantly with decreasing temperature, behavior that is characteristic of TADF compounds. The lifetimes of both PF and DF were estimated by fitting the decays with a multi-exponential decay fitting (for details of the fitting of the decays see page S4, ESI). The prompt, τ_p , and delayed, τ_d , lifetimes are $\tau_p/\tau_d = 6.83$ ns/13.72 μ s and 5.09 ns/95.91 μ s for **DIDOBNA-N** and **MesB-DIDOBNA-N**, respectively. Both emitters exhibited high radiative rates in the order of 10^8 s⁻¹ (Table 1); however, RISC rates are slow at 3.14×10^4 s⁻¹ and 9.81×10^3 s⁻¹, respectively for **DIDOBNA-N** and **MesB-DIDOBNA-N**; deep blue D-A DOBNA-containing TADF compounds have been reported to show k_{RISC} on average on the order of 10^6 s⁻¹.^{22, 23, 24, 25, 26, 27, 28, 45} More generally, deep blue MR-TADF compounds rarely show k_{RISC} above 10^4 s⁻¹.^{50, 51, 52} The

k_{RISC} for **DOBNA** was reported to be $1.6 \times 10^4 \text{ s}^{-1}$ in 1 wt% PMMA,²⁰ which is just slightly faster than that of **MesB-DIDOBNA-N** ($9.81 \times 10^3 \text{ s}^{-1}$).

Device performance

The potential of the emitters in deep-blue and violet electroluminescent (EL) devices was next assessed. To confine the excitons on the emitter, the high triplet energy material TSP01 was selected as the host. Since TSP01 has a dominant electron-transport character, the recombination zone inside the emission layer (EML) is believed to be located near the interface between the emission layer (EML) and the hole transport layer (HTL). To avoid exciton loss into the HTL, an exciton blocking layer of 10 nm thick CzSi [(9-(4-*tert*-butylphenyl)-3,6-bis(triphenylsilyl)-9*H*-carbazole, $E_{\text{T}} = 3.0 \text{ eV}$)]⁵³ was inserted between the EML and HTL. Furthermore, the doping concentration (c_{D} : 1.5 wt% - 5.0 wt%) of the emitter was carefully tuned investigate its effects on device performance and color purity.

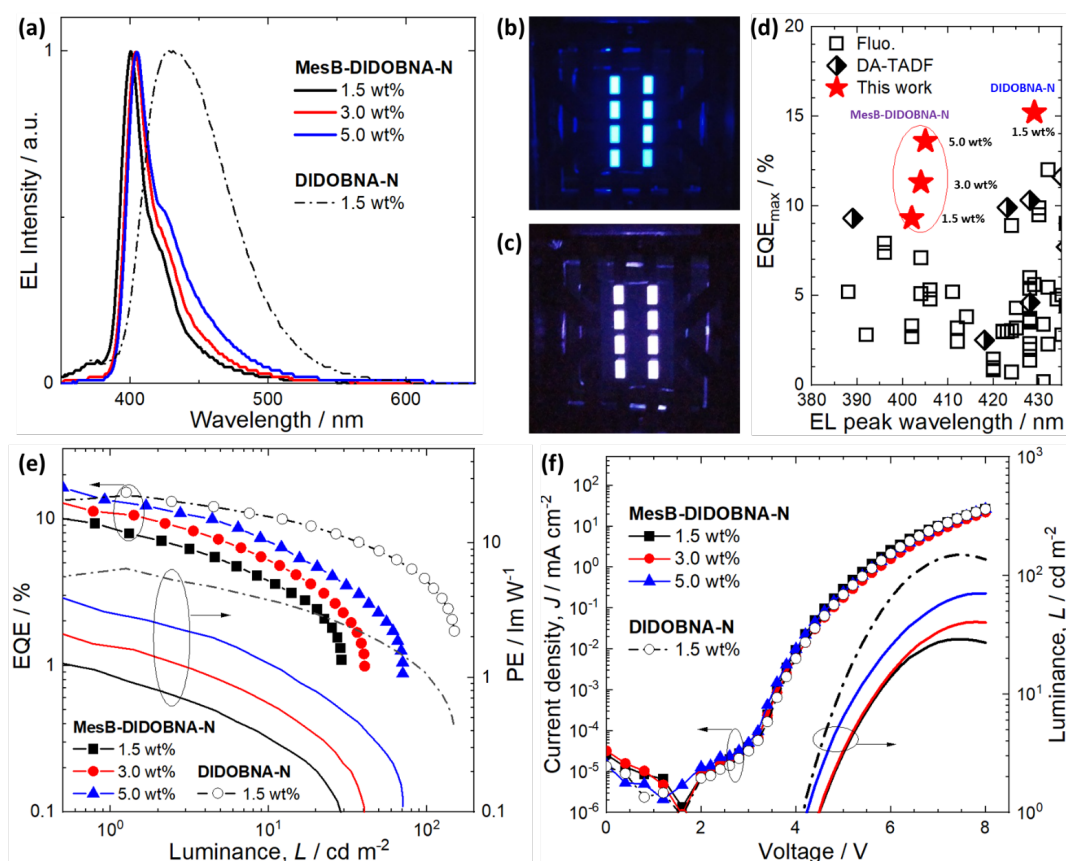


Figure 6. OLED device data for **MesB-DIDOBNA-N** and **DIDOBNA-N** as emitters. **a)** EL spectrum of both emitters at 5 V. **b)** and **c)** are images of operating devices of **DIDOBNA-N** and **MesB-DIDOBNA-N**, respectively under 5 V. **d)** EQE_{max} comparison in terms of EL peak wavelength of present emitters to reported fluorescent (Fluo.), and D-A-TADF emitters in OLEDs. Source references for

the plotted data are given in Table S7. e) Dependence of external quantum efficiency (EQE) and power efficiency (PE) on the luminance. f) Current density-voltage-luminance (J - V - L) characteristics of the device.

Using either of the emitters, the optimized device structure was: indium tin oxide (ITO)/hexaazatriphenylenehexacarbonitrile (HAT-CN, 5 nm)/ N,N' -di(1-naphthyl)- N,N' -diphenyl-(1,1'-biphenyl)-4,4'-diamine (NPB, 40 nm)/tris(4-carbazoyl-9-ylphenyl)amine (TCTA, 10 nm)/CzSi (10 nm)/ **MesB-DIDOBNA-N** or **DIDOBNA-N** or:TSPO1 (c_D , 20 nm)/TSPO1 (10 nm)/ 1,3,5-tris(3-pyridyl-3-phenyl)benzene (TmPyPB, 20 nm)/LiF (0.8 nm)/Al (100 nm), where HAT-CN, NPB, TCTA, CzSi, TSPO1, TmPyPB, LiF are the hole injection (HIL), hole transport (HTL), electron blocking (EBL), exciton blocking, hole blocking (HBL), electron transport (ETL), and electron injection layers (EIL), respectively. The device structure and energy levels of each layer are illustrated in Figure S20.

Focusing first on the OLEDs with **MesB-DIDOBNA-N**, both device efficiency and color purity depend sensitively on the doping concentration (c_D) of the emitter. To identify the optimum emitter doping level, devices were fabricated at different doping concentrations of **MesB-DIDOBNA-N** from 1.5 to 3.0 to 5.0 wt%. High c_D devices presented lower turn-on voltage (V_{on} , voltage at 1 cd m⁻²), higher brightness, higher maximum external quantum efficiency (EQE_{max}), and higher power efficiency (PE) as shown in Figure 6 and Table 2. At the lowest doping level of 1.5 wt%, the EL peak ($\lambda_{EL} = 402$, FWHM = 22 nm) was nearly identical to the λ_{PL} in dilute THF solution ($\lambda_{PL} = 399$ nm, FWHM = 23 nm). Figure 6a shows the EL spectrum of **MesB-DIDOBNA-N**, which is the bluest of all the MR-TADF OLEDs reported to date.^{10,11} In addition, the **MesB-DIDOBNA-N** devices exhibited the shortest λ_{EL} and narrowest FWHM among the reported purely organic molecule-based violet OLEDs.^{10,11} With increasing of c_D , the λ_{EL} red-shifted slightly to 404 nm (3wt%) and 405 nm (5wt%) while the FWHM increased to 25 nm and 31 nm, respectively. The spectral broadening resulted mainly from the increase in intensity of the low energy shoulder peak at 430 nm. Despite these undesired spectral changes with increasing c_D , devices showed extraordinary color purity, with CIE coordinates of (0.165, 0.044), (0.166, 0.045), and (0.166, 0.055) for the **MesB-DIDOBNA-N** OLEDs with c_D of 1.5, 3, and 5wt%, respectively. Those values, especially that with c_D of 3 wt%, are very close to the BT.2020 standard for the primary blue color of UHD TV [i.e., CIE coordinates of (0.131, 0.046)].

Considering the HOMO/LUMO levels of the emitter, **MesB-DIDOBNA-N** (5.73 eV/2.24 eV) and the host, TSPO1 (6.79 eV/2.50 eV), holes and electrons are mainly transported *via* the emitter and the host molecules, respectively. In other words, the injected holes are mostly trapped on the emitters, which then capture the mobile electrons hopping via the transporting sites of the TSPO1 host, i.e., the trap-assisted recombination mechanism. Therefore, at a low c_D of 1.5 wt%, it has a certain percentage of electrons that can migrate through the EML without being transferred to the emitters, which then leak into the TCTA layer and induce EL there. Indeed, EL at around 380 nm was observed in **MesB-DIDOBNA-N** device, which was attributed to the emission from TCTA. When the c_D is above 3 wt%, sufficient recombination is achieved, and the EL originates only from **MesB-DIDOBNA-N**. The EQE_{max} increased from 9.3 to 11.3 and 13.6% for the devices with emitter c_D of 1.5, 3.0 and 5.0 wt%, respectively (Figure 6e). The **MesB-DIDOBNA-N** OLED has the highest EQE_{max} among all the reported fluorescent and TADF emitters with λ_{EL} around 400 nm (Figure 6d and Table S7). It is noted that the maximum luminance (L_{max}) of the device is limited by the severe efficiency roll-off, which is attributed to a combination of carrier imbalance commonly observed in devices with low emitter doping in combination with high-energy band gap hosts and long-lived triplets that lead to an enhanced probability for bimolecular annihilation processes such as singlet-triplet annihilation, triplet-triplet annihilation processes, and triplet-polaron quenching.^{54, 55} Low L_{max} is endemic in deep blue TADF OLEDs with similar CIE_y values, such as devices with **tDIDCz** ($\text{CIE}_y = 0.02$) of 200 cd m^{-2} at 8 V,²⁹ **DCzBN1** ($\text{CIE}_y = 0.05$) of 320 cd m^{-2} at 10 V,⁵⁶ **B-O-dpa** ($\text{CIE}_y = 0.05$) of 180 cd m^{-2} at 8 V,⁵⁷ and **tBuOBOtSAc** ($\text{CIE}_y = 0.06$) of 350 cd m^{-2} at 12 V,²⁶ implying that factors other than the nature of the emitter need to be addressed in order to improve device performance, such as the stability of high triplet-energy host materials and the device structure.

The A-D-A compound **DIDOBNA-N** also presented a highly desirable set of photophysical properties in TSPO1. Using the same device structure as that of **MesDIDOBNA-N**, the OLED with **DIDOBNA-N** showed deep-blue unstructured EL ($\lambda_{\text{EL}} = 429$ nm, FWHM = 70 nm, CIE = 0.152, 0.073) at c_D of 1.5 wt% (Figure 6a), which corresponds well to the NTSC standard of (0.14, 0.08) for blue emission. Interestingly, The peak of the EL of **DIDOBNA-N** at 429 nm is close to the PL peak in dilute THF

solutions (426 nm), although the EL spectrum is broader. The V_{on} was 4.2 V, and the EQE_{max} was high at 15.2%, which decreased to 3.8% at 100 cd m^{-2} . Like the **MesB-DIDOBNA-N** OLED, the **DIDOBNA-N** device is among the most efficient devices at this λ_{EL} (Figure 6d and Table S7).^{10, 11}

Table 2. Device performance of **DIDOBNA-N** and **MesB-DIDOBNA-N**.

Emitter	$c_{\text{D}} / \text{wt}\%$	V_{on} / V	$\lambda_{\text{EL}} / \text{nm}$	FWHM / nm	CIE (x,y)	EQE_{max} ($\text{EQE}_{100\text{cd m}^{-2}} / \text{PE}_{\text{max}}$ % / lm W^{-1})
DIDOBNA-N	1.5	4.2	429	70	(0.152, 0.073)	15.2 (3.8) / 6.46
MesB-DIDOBNA-N	1.5	4.5	402	22	(0.165, 0.044)	9.3 (-) / 1.14
	3.0	4.5	404	25	(0.166, 0.045)	11.3 (-) / 1.78
	5.0	4.2	405	31	(0.165, 0.055)	13.6 (-) / 3.08

Conclusions

Two new easy-to-access TADF emitters have been synthesised in good yields. The A-D-A emitter **DIDOBNA-N** showed efficient pure blue emission and TADF in 1.5 wt% TSPO1 films ($\lambda_{\text{PL}} = 444 \text{ nm}$, FWHM = 64 nm, $\Phi_{\text{PL}} = 81\%$, $\tau_{\text{d}} = 23 \mu\text{s}$). The electroluminescence is blue-shifted ($\lambda_{\text{EL}} = 429 \text{ nm}$, FWHM = 70 nm, $\text{CIE}_y = 0.073$), corresponding well to the NTSC standard of (0.14, 0.08). The OLED shows an excellent EQE_{max} of 15.3%, which is the highest reported for a deep blue emitter with a $\lambda_{\text{EL}} < 430 \text{ nm}$.^{10, 25} The MR-TADF emitter, **MesB-DIDOBNA-N** was obtained from **DIDOBNA-N** in one step by installing a bridging mesitylated borane unit. This compound represents a rare example of a non triangulene type π -extended violet MR-TADF emitter. The molecular design utilized two electronically distinct acceptor boron atoms in combination with mixed donor nitrogen, and oxygen atoms. This emitter shows narrowband pure violet emission in the 1.5 wt% TSPO1 film ($\lambda_{\text{PL}} = 402 \text{ nm}$, FWHM = 19 nm, $\Phi_{\text{PL}} = 75\%$, $\tau_{\text{d}} = 133 \mu\text{s}$), which translated into record-setting near UV MR-TADF OLED EQE_{max} of 9.3%, ($\lambda_{\text{EL}} = 402 \text{ nm}$, FWHM = 22 nm, $\text{CIE}_y = 0.044$). The EL from the **MesB-DIDOBNA-N** device is the bluest of all the MR-TADF OLEDs reported to date.^{10, 11} Notably, the CIE_y value of the

MesB-DIDOBNA-N device is very close to the Rec.2020 standard for blue of (0.131, 0.046). The EQ_{max} value of the **MesB-DIDOBNA-N** device could be enhanced to 13.6% by increasing the doping concentration of the emitter to 5 wt%.¹¹

Supporting Information

¹H NMR and ¹³C NMR spectra, GCMS, HRMS and reverse phase and gel permeation (GPC) HPLC; supplementary computational data and coordinates; Crystallographic data (CIF). **DOBNA-Br** (CCDC 2171188); **DIDOBNA-N** (CCDC 2171190); **MesB-DIDOBNA-N** (CCDC 2171189). Additional photophysical and OLED data.

Acknowledgments

This project has received funding from the European Union's Horizon 2020 research and innovation programme under the Marie Skłodowska Curie grant agreement No 838885 (NarrowbandSSL). S.M.S. acknowledges support from the Marie Skłodowska-Curie Individual Fellowship (grant agreement No 838885 NarrowbandSSL). We would like to thank the Leverhulme Trust (RPG-2016-047) for financial support. E.Z-C. and I.D.W.S acknowledge support from EPSRC (EP/L017008, EP/P010482/1). Computational resources have been provided by the Consortium des Équipements de Calcul Intensif (CÉCI), funded by the Fonds de la Recherche Scientifiques de Belgique (F. R. S.-FNRS) under Grant No. 2.5020.11, as well as the Tier-1 supercomputer of the Fédération Wallonie-Bruxelles, infrastructure funded by the Walloon Region under the grant agreement n1117545. Y.O. acknowledges funding by the Fonds de la Recherche Scientifique-FNRS under Grant n° F.4534.21 (MIS-IMAGINE). D.B. is a FNRS Research Director.

References

1. Hong G, Gan X, Leonhardt C, Zhang Z, Seibert J, Busch JM, *et al.* A Brief History of OLEDs—Emitter Development and Industry Milestones. *Adv Mater* 2021, **33**(9): 2005630.
2. Parameter values for ultra-high definition television systems for production and international programme exchange *BT2020-2 (10/2015)*: International Telecommunication Union; 2015.

3. Cai X, Su S-J. Marching Toward Highly Efficient, Pure-Blue, and Stable Thermally Activated Delayed Fluorescent Organic Light-Emitting Diodes. *Adv Funct Mater* 2018, **28**(43): 1802558.
4. Fu H, Cheng Y-M, Chou P-T, Chi Y. Feeling blue? Blue phosphors for OLEDs. *Mater Today* 2011, **14**(10): 472-479.
5. Wong MY, Zysman-Colman E. Purely Organic Thermally Activated Delayed Fluorescence Materials for Organic Light-Emitting Diodes. *Adv Mater* 2017, **29**(22): 1605444.
6. Aizawa N, Matsumoto A, Yasuda T. Thermal equilibration between singlet and triplet excited states in organic fluorophore for submicrosecond delayed fluorescence. *Sci Adv* 2021, **7**(7): eabe5769.
7. Lee H, Karthik D, Lampande R, Ryu JH, Kwon JH. Recent Advancement in Boron-Based Efficient and Pure Blue Thermally Activated Delayed Fluorescence Materials for Organic Light-Emitting Diodes. *Front Chem* 2020, **8**.
8. Madayanad Suresh S, Hall D, Beljonne D, Olivier Y, Zysman-Colman E. Multiresonant Thermally Activated Delayed Fluorescence Emitters Based on Heteroatom-Doped Nanographenes: Recent Advances and Prospects for Organic Light-Emitting Diodes. *Adv Funct Mater* 2020, **30**(33): 1908677.
9. Huang J-W, Hsu Y-C, Wu X, Wang S, Gan X-Q, Zheng W-Q, *et al.* Influence of charge transfer strength on emission bandwidth for multiple-resonance emitters via systematically tuning the acceptor–donor assembly. *J Mater Chem C* 2022, **10**(20): 7866-7874.
10. Ha JM, Hur SH, Pathak A, Jeong J-E, Woo HY. Recent advances in organic luminescent materials with narrowband emission. *NPG Asia Mater* 2021, **13**(1): 53.
11. Chen S, Xu H. Electroluminescent materials toward near ultraviolet region. *Chem Soc Rev* 2021, **50**(15): 8639-8668.
12. Shinar J, Shinar R. Organic light-emitting devices (OLEDs) and OLED-based chemical and biological sensors: an overview. *J Phys D: Appl Phys* 2008, **41**(13): 133001.
13. Thakare DS, Omanwar SK, Muthal PL, Dhopte SM, Kondawar VK, Moharil SV. UV-emitting phosphors: synthesis, photoluminescence and applications. *Phys Status Solidi A* 2004, **201**(3): 574-581.
14. Santen HV, Neijzen JHM. Deep-UV Liquid Immersion Mastering of High Density Optical Discs. *Jpn J Appl Phys* 2003, **42**(Part 1, No. 2B): 1110-1112.

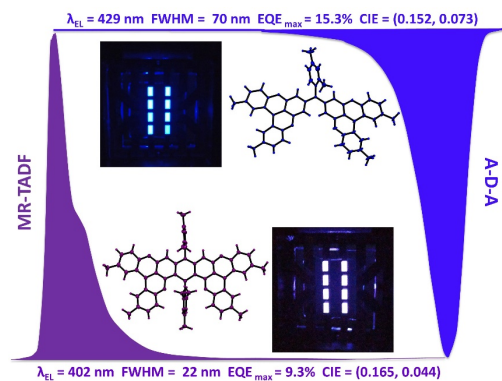
15. Thi Tuyet Nhung L, Nagata H, Takahashi A, Aihara M, Okamoto T, Shimohata T, *et al.* Sterilization effect of UV light on *Bacillus* spores using TiO₂ films depends on wavelength. *J Med Invest* 2012, **59**(1,2): 53-58.
16. Zhang H, Li G, Guo X, Zhang K, Zhang B, Guo X, *et al.* High-Performance Ultraviolet Organic Light-Emitting Diode Enabled by High-Lying Reverse Intersystem Crossing. *Angew Chem Int Ed* 2021, **60**(41): 22241-22247.
17. Chen J, Liu H, Guo J, Wang J, Qiu N, Xiao S, *et al.* Robust Luminescent Molecules with High-Level Reverse Intersystem Crossing for Efficient Near Ultraviolet Organic Light-Emitting Diodes. *Angew Chem Int Ed* 2022, **61**(10): e202116810.
18. Xu Y, Xu P, Hu D, Ma Y. Recent progress in hot exciton materials for organic light-emitting diodes. *Chem Soc Rev* 2021, **50**(2): 1030-1069.
19. Hirai H, Nakajima K, Nakatsuka S, Shiren K, Ni J, Nomura S, *et al.* One-Step Borylation of 1,3-Diaryloxybenzenes Towards Efficient Materials for Organic Light-Emitting Diodes. *Angew Chem Int Ed* 2015, **54**(46): 13581-13585.
20. Ikeda N, Oda S, Matsumoto R, Yoshioka M, Fukushima D, Yoshiura K, *et al.* Solution-Processable Pure Green Thermally Activated Delayed Fluorescence Emitter Based on the Multiple Resonance Effect. *Adv Mater* 2020, **32**(40): 2004072.
21. Liang D, Peng Y, Fu Y, Shearer MJ, Zhang J, Zhai J, *et al.* Color-Pure Violet-Light-Emitting Diodes Based on Layered Lead Halide Perovskite Nanoplates. *ACS Nano* 2016, **10**(7): 6897-6904.
22. Ahn DH, Kim SW, Lee H, Ko IJ, Karthik D, Lee JY, *et al.* Highly efficient blue thermally activated delayed fluorescence emitters based on symmetrical and rigid oxygen-bridged boron acceptors. *Nat Photonics* 2019, **13**(8): 540-546.
23. Kim HJ, Godumala M, Kim SK, Yoon J, Kim CY, Park H, *et al.* Color-Tunable Boron-Based Emitters Exhibiting Aggregation-Induced Emission and Thermally Activated Delayed Fluorescence for Efficient Solution-Processable Nondoped Deep-Blue to Sky-Blue OLEDs. *Adv Opt Mater* 2020, **8**(14): 1902175.
24. Lim H, Cheon HJ, Woo S-J, Kwon S-K, Kim Y-H, Kim J-J. Highly Efficient Deep-Blue OLEDs using a TADF Emitter with a Narrow Emission Spectrum and High Horizontal Emitting Dipole Ratio. *Adv Mater* 2020, **32**(47): 2004083.
25. Hwang J, Koh CW, Ha JM, Woo HY, Park S, Cho MJ, *et al.* Aryl-Annulated [3,2-a] Carbazole-Based Deep-Blue Soluble Emitters for High-Efficiency Solution-Processed Thermally Activated Delayed Fluorescence Organic Light-Emitting Diodes with CIEy <0.1. *ACS Appl Mater Interfaces* 2021, **13**(51): 61454-61462.

26. Lee Y, Hong J-I. High-Efficiency Thermally Activated Delayed Fluorescence Emitters with High Horizontal Orientation and Narrow Deep-Blue Emission. *Adv Opt Mater* 2021, **9**(15): 2100406.
27. Tan H-J, Yang G-X, Deng Y-L, Cao C, Tan J-H, Zhu Z-L, *et al.* Deep-Blue OLEDs with Rec.2020 Blue Gamut Compliance and EQE Over 22% Achieved by Conformation Engineering. *Adv Mater*, **n/a**(n/a): 2200537.
28. Gan Y, Peng X, Qiu W, Wang L, Li D, Xie W, *et al.* Multiple charge transfer disk-like emitters with fast fluorescence radiation rate and high horizontal dipole orientation for pure blue organic light-emitting diodes. *Chem Eng J* 2022, **430**: 133030.
29. Lee HL, Chung WJ, Lee JY. Narrowband and Pure Violet Organic Emitter with a Full Width at Half Maximum of 14 nm and y Color Coordinate of Below 0.02. *Small* 2020, **16**(14): 1907569.
30. Hall D, Stavrou K, Duda E, Danos A, Bagnich S, Warriner S, *et al.* Diindolocarbazole – achieving multiresonant thermally activated delayed fluorescence without the need for acceptor units. *Mater Horiz* 2022, **9**(3): 1068-1080.
31. Suresh SM, Duda E, Hall D, Yao Z, Bagnich S, Slawin AMZ, *et al.* A Deep Blue B,N-Doped Heptacene Emitter That Shows Both Thermally Activated Delayed Fluorescence and Delayed Fluorescence by Triplet–Triplet Annihilation. *J Am Chem Soc* 2020, **142**(14): 6588-6599.
32. K. Stavrou, S. M. Suresh, D. Hall, A. Danos, N. Kukhta, A. Slawin, *et al.* Emission and Absorption Tuning in MR-TADF B,N-Doped Hep-tacenes: Towards Ideal-Blue Hyperfluorescent OLEDs. *ChemRxiv preprint DOI: 1026434/chemrxiv-2022-5hg9*; 2022.
33. Agou T, Kobayashi J, Kawashima T. Syntheses, Structure, and Optical Properties of Ladder-Type Fused Azaborines. *Org Lett* 2006, **8**(11): 2241-2244.
34. D. Hall, J. C. Sancho, A. Pershin, D. Beljonne, E. Zysman-Colman, Y. Olivier. The modelling of multi-resonant thermally activated delayed fluorescence emitters – properly accounting for electron correlation is key! *ChemRxiv preprint DOI: 1026434/chemrxiv8091314v1*; 2021.
35. Etherington MK, Gibson J, Higginbotham HF, Penfold TJ, Monkman AP. Revealing the spin–vibronic coupling mechanism of thermally activated delayed fluorescence. *Nat Commun* 2016, **7**(1): 13680.
36. Hempe M, Kukhta NA, Danos A, Fox MA, Batsanov AS, Monkman AP, *et al.* Vibrational Damping Reveals Vibronic Coupling in Thermally Activated Delayed Fluorescence Materials. *Chem Mater* 2021, **33**(9): 3066-3080.
37. Luo X-F, Ni H-X, Ma H-L, Qu Z-Z, Wang J, Zheng Y-X, *et al.* Fused π -Extended Multiple-Resonance Induced Thermally Activated Delayed Fluorescence Materials for High-Efficiency and Narrowband OLEDs with Low Efficiency Roll-Off. *Adv Opt Mater* 2022, **10**(9): 2102513.

38. Patil VV, Lee HL, Kim I, Lee KH, Chung WJ, Kim J, *et al.* Purely Spin-Vibronic Coupling Assisted Triplet to Singlet Up-Conversion for Real Deep Blue Organic Light-Emitting Diodes with Over 20% Efficiency and γ Color Coordinate of 0.05. *Advanced Science* 2021, **8**(20): 2101137.
39. Olivier Y, Sancho-Garcia JC, Muccioli L, D'Avino G, Beljonne D. Computational Design of Thermally Activated Delayed Fluorescence Materials: The Challenges Ahead. *The Journal of Physical Chemistry Letters* 2018, **9**(20): 6149-6163.
40. Connelly NG, Geiger WE. Chemical Redox Agents for Organometallic Chemistry. *Chem Rev* 1996, **96**(2): 877-910.
41. Song D, Yu Y, Yue L, Zhong D, Zhang Y, Yang X, *et al.* Asymmetric thermally activated delayed fluorescence (TADF) emitters with 5,9-dioxa-13b-boranaphtho[3,2,1-de]anthracene (OBA) as the acceptor and highly efficient blue-emitting OLEDs. *J Mater Chem C* 2019, **7**(38): 11953-11963.
42. Ahn DH, Maeng JH, Lee H, Yoo H, Lampande R, Lee JY, *et al.* Rigid Oxygen-Bridged Boron-Based Blue Thermally Activated Delayed Fluorescence Emitter for Organic Light-Emitting Diode: Approach towards Satisfying High Efficiency and Long Lifetime Together. *Adv Opt Mater* 2020, **8**(11): 2000102.
43. Melhuish WH. Quantum Efficiencies of Fluorescence of Organic Substances: Effect of Solvent and Concentration of The Fluorescent Solute1. *J Phys Chem* 1961, **65**(2): 229-235.
44. Tsuchiya Y, Diesing S, Bencheikh F, Wada Y, dos Santos PL, Kaji H, *et al.* Exact Solution of Kinetic Analysis for Thermally Activated Delayed Fluorescence Materials. *J Phys Chem A* 2021, **125**(36): 8074-8089.
45. Park IS, Min H, Kim JU, Yasuda T. Deep-Blue OLEDs Based on Organoboron–Phenazasiline-Hybrid Delayed Fluorescence Emitters Concurrently Achieving 30% External Quantum Efficiency and Small Efficiency Roll-Off. *Adv Opt Mater* 2021, **9**(24): 2101282.
46. Lakowicz JR. Quenching of Fluorescence. In: Lakowicz JR (ed). *Principles of Fluorescence Spectroscopy*. Springer US: Boston, MA, 1983, pp 257-301.
47. Jeon SO, Jang SE, Son HS, Lee JY. External Quantum Efficiency Above 20% in Deep Blue Phosphorescent Organic Light-Emitting Diodes. *Adv Mater* 2011, **23**(12): 1436-1441.
48. Northey T, Stacey J, Penfold TJ. The role of solid state solvation on the charge transfer state of a thermally activated delayed fluorescence emitter. *J Mater Chem C* 2017, **5**(42): 11001-11009.

49. Serevičius T, Skaisgiris R, Dodonova J, Fiodorova I, Genevičius K, Tumkevičius S, *et al.* Temporal Dynamics of Solid-State Thermally Activated Delayed Fluorescence: Disorder or Ultraslow Solvation? *J Phys Chem Lett* 2022, **13**(7): 1839-1844.
50. Nagata M, Min H, Watanabe E, Fukumoto H, Mizuhata Y, Tokitoh N, *et al.* Fused-Nonacyclic Multi-Resonance Delayed Fluorescence Emitter Based on Ladder-Thiaborin Exhibiting Narrowband Sky-Blue Emission with Accelerated Reverse Intersystem Crossing. *Angew Chem Int Ed* 2021, **60**(37): 20280-20285.
51. Oda S, Kawakami B, Yamasaki Y, Matsumoto R, Yoshioka M, Fukushima D, *et al.* One-Shot Synthesis of Expanded Heterohelicene Exhibiting Narrowband Thermally Activated Delayed Fluorescence. *J Am Chem Soc* 2022, **144**(1): 106-112.
52. Bian J, Chen S, Qiu L, Tian R, Man Y, Wang Y, *et al.* Ambipolar Self-Host Functionalization Accelerates Blue Multi-Resonance Thermally Activated Delayed Fluorescence with Internal Quantum Efficiency of 100%. *Adv Mater*, n/a(n/a): 2110547.
53. Tsai M-H, Ke T-H, Lin H-W, Wu C-C, Chiu S-F, Fang F-C, *et al.* Triphenylsilyl- and Trityl-Substituted Carbazole-Based Host Materials for Blue Electrophosphorescence. *ACS Appl Mater Interfaces* 2009, **1**(3): 567-574.
54. van der Zee B, Li Y, Wetzelaer G-JAH, Blom PWM. Numerical Device Model for Organic Light-Emitting Diodes Based on Thermally Activated Delayed Fluorescence. *Advanced Electronic Materials* 2022, **8**(7): 2101261.
55. Hasan M, Saggarr S, Shukla A, Bencheikh F, Sobus J, McGregor SKM, *et al.* Probing polaron-induced exciton quenching in TADF based organic light-emitting diodes. *Nat Commun* 2022, **13**(1): 254.
56. Chan CY, Cui LS, Kim JU, Nakanotani H, Adachi C. Rational Molecular Design for Deep-Blue Thermally Activated Delayed Fluorescence Emitters. *Adv Funct Mater* 2018, **28**(11): 1706023.
57. Park J, Lim J, Lee JH, Jang B, Han JH, Yoon SS, *et al.* Asymmetric Blue Multiresonance TADF Emitters with a Narrow Emission Band. *ACS Appl Mater Interfaces* 2021, **13**(38): 45798-45805.

TOC graphic



Transformation of a deep-blue acceptor-donor-acceptor TADF emitter, DIDOBNA-N, to a multiresonant TADF emitter, MesB-DIDOBNA-N is demonstrated. Efficient deep-blue OLEDs with EQE_{max} and CIE_y ordinate of 15.3% and 0.073 with **DIDOBNA-N** and 9.3% and 0.044 with **MesB-DIDOBNA-N** illustrate the promise of the molecular design of these emitters.